Two-Dimensional Micromachined Flow Sensor Array for Fluid Mechanics Studies

Jack Chen[1]; Zhifang Fan[2]; Jun Zou[3]; Jonathan Engel[4]; and Chang Liu[5]

Abstract: We discuss two types of micromachined flow sensors realized by using novel microfabrication processes—a hot-wire anemometer (based on thermal transfer) and a biologically inspired flow sensor (based on momentum transfer). Both sensors are enabled by a new, efficient three-dimensional assembly technique called the plastic deformation magnetic assembly method. The sensors can be packaged in high-density, two-dimensional arrays efficiently, with each sensor node capable of performing two-component or three-component flow sensing. We first discuss the development of new hot-wire anemometers (HWA). The HWA uses a thermal element (hot wire) that is made of Pt/Ni/Pt film with a measured temperature coefficient of resistance of 2,700 ppm/°C. The thermal element is elevated out of plane by using support beams made of polyimide, a polymer material. Both steady-state and transient characteristics of the sensor have been experimentally obtained. The second type of flow sensor is based on momentum transfer principles and inspired by fish lateral line sensors. Each sensor consists of a vertical cilium attached to a horizontal cantilever. Fluid flow imparts moment on the vertical cilium, and causes the horizontal cantilever to bend. The fabrication process and preliminary measurement data are presented.

DOI: 10.1061/(ASCE)0893-1321(2003)16:2(85)

CE Database subject headings: Sensors; Fluid mechanics; Fluid flow.

Introduction

Flow sensors for fluid mechanics studies must satisfy a number of performance requirements, such as multicomponent, vector flow sensing, fast response speed, low-detection limit, least intrusion to the flow field of interests, and preferably low costs. For certain applications, it is also desirable that high-density, two-dimensional arrays of such sensors can be made for boundary-layer flow studies.

Many engineered flow sensors have been developed in the past based on a number of sensing principles, including thermal anemometry (e.g., hot-wire or hot-film anemometers) (Perry 1982), Doppler frequency shift, and indirect inference from pressure differences (Rediniotis 1999; Richter et al. 1999). A hot-wire or hot-film anemometer uses flow-induced, forced convection to indirectly infer the flow rate. The majority of existing hot-wire anemometers are made using conventional machining methods. Sensors based on Doppler frequency shifts consist of an acoustic launcher and a receiver. The sizes of such sensor devices are generally large.

In the past two decades, several research groups have developed micromachined flow sensors (Kovacs 1998) that are based on a variety of sensing principles, including the three major principles mentioned above. Microfabrication offers the benefits of high-spatial resolution, fast time response (due to low mass and thermal mass), integrated signal processing, and potentially low costs. Using microphotolithography, it is cost efficient to make large arrays of sensors with good uniformity. Microsensors based on various principles including thermal transfer (Lofdahl et al. 1992; van der Wiel et al. 1993; Jiang et al. 1994; Ebefors et al. 1998; de Bre et al. 1999; van Honschoten et al. 2001; van Baar et al. 2001), torque transfer (van der Weil et al. 1995; Enoksson et al. 1996; Svedin et al. 1998; Svedin et al. 2001), and pressure distribution (Boillat et al. 1995; Kalvesten et al. 1996; Lofdahl et al. 1996) have been demonstrated. In addition to flow sensors, boundary-layer shear stress sensors have been realized using floating element methods (Padmanabhan et al. 1996) and thermal transfer principles (Xu et al. 2002). However, shear stress sensors are located directly on the fluid-solid boundary and do not provide true sensitivity to flow rates.

There remain a number of challenges for realizing arrayed, high-sensitivity, and low-cost flow sensors. We discuss the development of two types of new flow rate sensors made by micromachining methods, one based on thermal transfer principles and another based on momentum transfer principles. The basic motivation of our work is (1) to provide high-performance, low-cost sensors to fluid mechanics studies and (2) to demonstrate the feasibility of forming large two-dimensional array of flow sensors.

Three-Dimensional Assembly

Flow sensors invariably require sensing elements that are suspended in the flow media. This requirement poses an important

[1]Micro and Nanotechnology Laboratory, Univ. of Illinois at Urbana-Champaign, 208 North Wright Street, Urbana, IL 61801.

[2]Micro and Nanotechnology Laboratory, Univ. of Illinois at Urbana-Champaign, 208 North Wright Street, Urbana, IL 61801.

[3]Micro and Nanotechnology Laboratory, Univ. of Illinois at Urbana-Champaign, 208 North Wright Street, Urbana, IL 61801.

[4]Micro and Nanotechnology Laboratory, Univ. of Illinois at Urbana-Champaign, 208 North Wright Street, Urbana, IL 61801.

[5]Micro and Nanotechnology Laboratory, Univ. of Illinois at Urbana-Champaign, 208 North Wright Street, Urbana, IL 61801 (corresponding author). E-mail: changliu@uiuc.edu

Note. Discussion open until September 1, 2003. Separate discussions must be submitted for individual papers. To extend the closing date by one month, a written request must be filed with the ASCE Managing Editor. The manuscript for this paper was submitted for review and possible publication on November 6, 2002; approved on November 6, 2002. This paper is part of the ***Journal of Aerospace Engineering***, Vol. 16, No. 2, April 1, 2003. ©ASCE, ISSN 0893-1321/2003/2-85–97/$18.00.

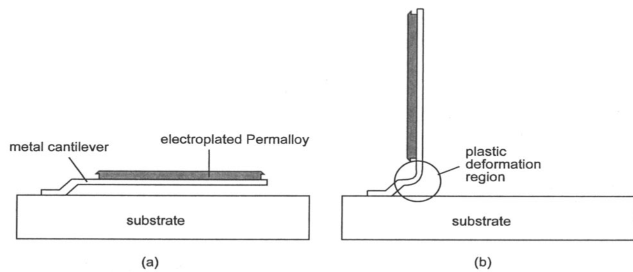

Fig. 1. Schematic diagram of PDMA process. (a) A representative cantilever with electroplated magnetic material attached and (b) magnetic actuation causes cantilever beam to rotate off substrate plane. Plastic deformation occurs near the anchor region.

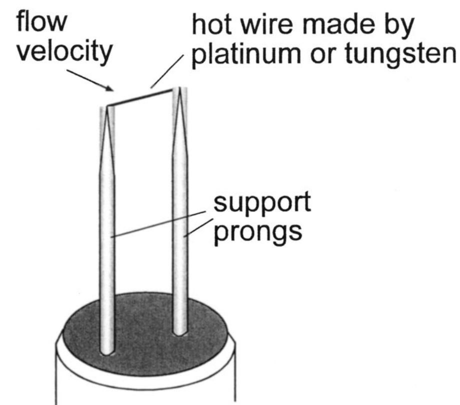

Fig. 2. Schematic diagram of conventional hot-wire anemometer

challenge to microfabrication. Researchers have primarily used silicon bulk micromachining to release flow-sensing elements by removing the underlying substrate material. However, there are important restrictions-associated with this method. Detailed discussions of deficiencies can be found in the sections, "Arrayed Hot-wire Anemometer—Introduction and Flow Sensors Based on Momentum Transfer—Introduction."

The sensors discussed in this paper are enabled by a new three-dimensional assembly technique called plastic deformation magnetic assembly (PDMA) (Zou et al. 2001). The principle of the assembly process is discussed as follows (Fig. 1). To illustrate the principle, we use a simple configuration that consists of a cantilever beam with a piece of electroplated magnetic material attached to it. The structure can be realized by using surface micromachining techniques. A thin-film sacrificial layer is first deposited and patterned. A metal thin film is evaporated and patterned, forming the cantilever beam. A piece of ferromagnetic material is electroplated on top of the cantilever. The cantilever beam, along with the magnetic piece, is subsequently released from the substrate by selectively etching the sacrificial layer [Fig. 1(a)]. The cantilever is attached to the substrate only at the anchor point. Subsequently, an external magnetic field is applied from underneath the substrate, bending the cantilever beam away from the substrate. If the amount of bending is above a certain threshold, the cantilever will be plastically deformed, resulting in permanent displacement [Fig. 1(b)]. The bent form is retained even after the magnetic field is removed.

The PDMA process offers a number of advantages. It avoids the use of bulk silicon micromachining and instead, uses more efficient surface micromachining techniques. It requires simple, low-temperature process steps and therefore is compatible with many materials (e.g., polymer substrate material). The assembly of many vertical structures can be achieved simultaneously using a global magnetic field, hence increasing the efficiency. The plastically bent cantilever naturally provides an electrical connection between the substrate and elevated microstructures.

In the following sections, we discuss the application of the PDMA assembly process in realizing two types of flow sensors.

Arrayed Hot-Wire Anemometer

Introduction

Hot-wire anemometry (HWA) utilizes a thermal element that serves as both a Joule heater and a temperature sensor. Under a constant bias power and zero flow rates, the thermal element assumes a steady-state temperature. If external fluid flow is present around the thermal element, the thermal element will experience forced convective cooling. Accordingly, the temperature of the thermal element will decrease, providing information on the flow rate, which governs the cooling rate.

Conventional hot-wire anemometers are noted for its low cost, fast response (in the range), small sizes, and low noise (Goldstein 1983). A HWA sensor is assembled individually by mounting a thin wire made of platinum or tungsten onto support prongs (Fig. 2). It is a common practice to thin the wire (e.g., by etching in acidic solutions) until the desired dimensions are reached (typically 1 mm long and a few micrometers in diameter). This active portion of the sensor is then mounted on a long probe with an electrical connection for ease of handling.

Conventional HWAs suffer from two major drawbacks (1) first, the fabrication and assembly process is delicate and does not guarantee uniformity of performance and (2) second, it is prohibitively difficult to form large arrays of HWA for measuring flow distribution. Arrays of HWAs each with multiple-component flow sensing capability is especially challenging.

In recent years, researchers have applied micromachining processes to realize HWA for airflow with smaller dimensions, better uniformity, and faster time response (due to smaller thermal masses possible). A representative strategy is to use the bulk-micromachining technique to produce freestanding cantilever structures. For example, researchers have reported making prongs and hot wires out of doped polycrystalline silicon and releasing the cantilever by partially removing the lightly doped silicon substrate (Jiang et al. 1994). One group used doped silicon for both the prong and the hot wire along with a polyimide hinge to make three-component hot-wire sensors (Ebefors et al. 1998). Another group undercut a polysilicon hot wire with wet etching so the hot wire is suspended over a cavity for better thermal insulation (Neda et al. 1996).

Almost all existing micromachined HWAs for airflow measurement use silicon as the thermal element and involve bulk micromachining of silicon to some extent, to our knowledge. Researchers have reported using a metal thermal element lying on polyimide bulk film (Dittmann et al. 2001); however, the lack of thermal isolation limits its use.

Existing micromachined hot-wire anemometers can be improved in a number of ways (1) silicon is an expensive substrate material. The cost of micromachined HWA would be reduced if the HWA can be made on nonsilicon substrates, (2) the process is complex and time consuming. The doping of silicon (e.g., for

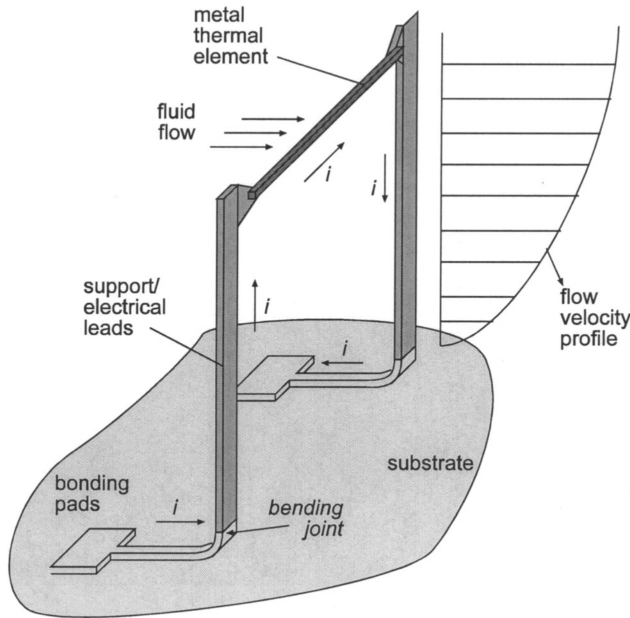

Fig. 3. Schematic diagram of a single out-of-plane HWA. Thermal element is made of metal thin film and supported by two support beams, which also provide electrical leads. Thermal element is elevated away from substrate surface (and bottom of velocity boundary layer.

creating hot wire) and the etching of silicon require significant expertise, facility, and efforts. Bulk etching using anisotropic wet etchants frequently pose concerns of materials compatibility as all materials on a given substrate are required to sustain wet etching for long periods (several hours to etch through typical silicon wafers). It would be advantageous if such time-consuming and high-cost process steps can be replaced, and (3) most of the micromachined HWAs are made as individual sensing nodes and cannot be realized in large array format efficiently. Bulk-micromachined HWA, for example, must be turned up right before it can be configured into a two-dimensional array. However, it is very difficult to package individual dies and make electrical connections.

Our research is motivated by the needs to further reduce the cost of micromachined HWA, to allow efficient fabrication and packaging, and to produce arrayed HWAs on potentially flexible substrates. We follow two fabrication strategies. First, we realize HWA by using surface micromachining in conjunction with three-dimensional assembly methods. This circumvents the use of time-consuming bulk-micromachining steps. Surface micromachining also enables more efficient assembly and allows formation of large arrays of HWAs. Second, we realize thermal elements using nonsilicon, temperature-sensitive materials. This could reduce costs as we avoid entirely the use of silicon bulk (as substrate) or thin film (as hot wire).

Sensor Design

The schematic diagram of the new out-of-plane anemometer is shown in Fig. 3. A thermal element is elevated from the substrate to a predetermined height that corresponds to the length of the support prongs. By elevating the thermal element away from the bottom of the velocity boundary layer, the thermal element experiences greater fluid flow velocity and exhibits greater sensitivity.

Table 1. Table of Material Property. All Values are Cited from Kovacs 1998 Except for Thermal Conductivity of Polyimide, Which is Cited from HD Microsystems 1998.

	Thermal coefficient of resistance or α_R (ppm)	Resistivity $(\mathrm{W\,cm}) \times 10^{-6}$	Thermal conductivity, k (W/cm °C)
Tungsten	4,500	4.2	1.73
Platinum	3,927	10.6	0.716
Nickel	6,900	6.84	0.91
Polyimide (PI 2611)	—	—	0.001–0.00357

The thermal element is electrically connected to the substrate through the support prongs as well.

The heat balance equation for the thermal element under electrical Joule heating is (Blackwelder 1981; Perry 1982; Lomas 1986)

$$Q_s = Q_{\mathrm{gen}} - Q_{\mathrm{conv}} - Q_{\mathrm{cond}} \tag{1}$$

where Q_s=rate of heat storage; Q_{gen}=generated (bias) power from Joule heating; Q_{conv}=rate of heat loss due to forced convection; and Q_{cond}=sum of conductive losses (e.g., through support prongs). Under a given set of Q_{gen} and fluid flow rate, it is important to minimize Q_{cond} in order to obtain greater sensitivity to velocity changes. To minimize the conductive heat loss also means that the HWA sensor can be operated in more thermally efficient manner, which is especially important if one were to operate a large array of such sensors. One reduces the conduction loss by supporting the thermal element using out-of-plane prongs that have high-aspect ratio, small cross section, and accordingly, relatively large thermal resistance.

The hot-wire consists of temperature-sensitive metal thin film on a supporting polyimide piece. We choose to have 2.7-μm-thick polyimide support because the thermal conductivity of polyimide is low, almost two orders of magnitude lower than that of a metal, e.g., nickel (see Table 1). The polyimide support provides needed structural rigidity without increasing the thermal conductivity. The thickness of the support should be decided by balancing several requirements. If the thickness is much lower than this value, the mechanical rigidity will likely be degraded. On the other hand, if the thickness is much greater, there is concern that the polyimide support will decrease the frequency response of the HWA due to added thermal mass.

The temperature of a hot wire can be inferred from the change of the resistance of the sensing element. The resistance (R) of a hot wire is linearly related to its temperature (T) to a first-order approximation

$$R = R_0[1 + \alpha(T - T_0)]] \tag{2}$$

where R_0=nominal resistance under a reference temperature T_0 (e.g., room temperature); and α=thermal coefficient of resistance (TCR) of the thermal element.

Optimal selection of the length of the hot wire (l_s) must balance both performance requirements (sensitivity) and fabrication requirements. It is possible to increase Q_{conv} relative to Q_{cond} by increasing the length of the hot wire (Brunn 1995). However, l_s is limited by fabrication practicality and yield considerations. The longer the thermal elements, the more difficult it is to realize such. Another important design parameter is the cross section of the hot wire. By reducing the value of the cross section, the surface-to-volume ratio of the hot wire is increased, hence encouraging more convection while confining the conductive com-

ponent. However, there exist a practical limit to the minimal diameter of the hot wire as well, due to mechanical rigidity concerns.

Our current study is aimed at establishing the fundamental design, process feasibility, and reliability. A wide range of dimensional parameters has been accommodated in our prototype design. Devices with hot-wire lengths of 50, 100, 150, and 200 μm, as well as heights of 400, 600, 800, and 1,000 μm were fabricated. The cross-section area of the hot wire is a 1,200-Å-thick metal film overlapping with a polyimide piece. The cross section of the polyimide piece is 6 μm wide by 2.7 μm thick. The cross section of the composite thermal element is comparable to that of commercially available hot wire sensors. Both the thermal element and the support prongs have a relatively small frontal area. The momentum imparted by fluid on the sensor is minimal. Because the sensor is at least partially immersed in the velocity boundary layer, it is possible to develop sensors that can withstand high-flow velocity by lowering its height and fully immersing it in the boundary layer.

Sensor Fabrication

Conventional HWAs use wires made of tungsten, platinum, or metal alloys as the sensing element. However, the thermal elements of our HWA are not made of exactly the same materials as conventional HWAs. Several candidate materials are evaluated (Table 1). Tungsten has a high-melting point and is difficult to deposit. Thin-film platinum does not have as high a temperature coefficient of resistance (TCR) value as thin-film Ni. Ni is the primary thermal element material used because the measured TCR value of deposited Ni thin films (approximately 4,100 ppm/°C) is high and the material process is relatively easy.

The overall fabrication process (Fig. 4) starts with a solid substrate. Because the process temperature is kept low, many substrate materials, including silicon, glass, and polymer, can be used. First, we evaporate and pattern a chrome/copper/titanium metal stack as the sacrificial layer [Fig. 4(a)]. The chrome film is 10-nm-thick and serves as the adhesion layer. The 250-Å-thick titanium thin film reduces the in-process oxidation of the 2,500-Å-thick copper film. We deposit a 2.7-μm-thick photodefinable polyimide (HD-4000) to form the support prongs and part of the hot wire. The film is patterned via lithography, and cured at 350°C [Fig. 4(b)] for 2 h. A Cr/Pt/Ni/Pt film is then evaporated and patterned to form the thermal element [Fig. 4(c)]. The Cr layer, serving as an adhesion layer, is 200 Å. A 800-Å-thick Ni resistor is sandwiched between two 200-Å-thick Pt films, which are used to reduce possible oxidation of Ni while in operation because Pt is relatively inert at high temperature of operations. We experimentally find that the TCR value of the composite thermal element (Cr/Pt/Ni/Pt film stack) is 2,700 ppm/°C between 25 and 100°C.

A 5,000-Å-thick Cr/Au film [Fig. 4(d)] is evaporated and patterned to serve as a mechanical bending element as well as electrical leads of the hot-wire filament. We electroplate a 4-μm-thick Permalloy thin film on portions of the cantilever support prongs [Fig. 4(e)] for PDMA assembly. The removal of the sacrificial layer (copper) is performed by using a solution containing acetic acid and hydrogen peroxide. PDMA assembly is carried out to lift the entire sensor out of plane [Figs. 4(f and h)] by placing a permanent magnet (field strength 800 gauss) at the bottom of the substrate.

We have strengthened the bent hinge such that the HWA can operate at high-flow speed. An additional postrelease Ni electroplating step is added. Ni (3–4 μm thick) is selectively electroplated at the bent hinges to strengthen the hinges (Fig. 5).

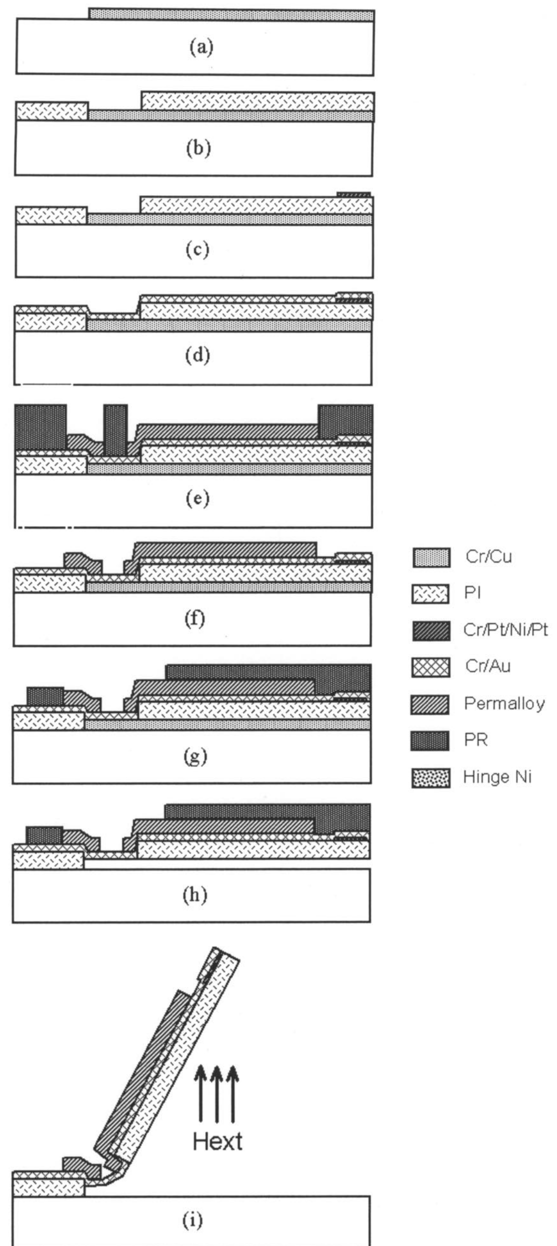

Fig. 4. Fabrication process of surface micromachined hot-wire anemometer (a) deposition of sacrificial layer, (b) pattern polyimide structure, (c) deposit nickel sensor, (d) deposit gold, (e) electroplate Permalloy, (f) strip electroplating mold, (g) pattern PR layer for postrelease plating, (h) sacrificial layer etching, and (i) PDMA assembly

A SEM micrograph of a representative device after release and assembly is shown in Fig. 6. Fig. 7 shows the scanning electron microscope (SEM) of the Au hinge with and without the postrelease plating. We have also demonstrated the ability to realize HWA with multiple-component sensing capability. A SEM of a three-component HWA is shown in Fig. 8. The HWA array can be fabricated on silicon, glass, or polymer substrates (e.g., liquid-crystal polymer and Kapton). This development could allow unprecedented ability to conducted boundary flow characterization experimentally.

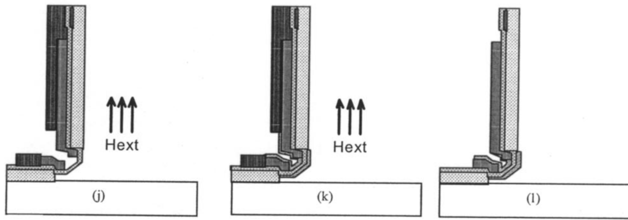

Fig. 5. Electroplating in bath under microscope to reinforce hinge: (a) device place in bath and external magnetic field applied to bring structure to 90°; (b) power supplied to hinge and start plating at ~2 mA for 5 min; and (c) once plating completed, remove sample from bath and strip resist

Steady-State Output Responses

We test the steady-state response of the sensors in a wind tunnel under both constant current and constant temperature modes. The fabricated hot-wire anemometer chip is attached to a PC board with etched wiring traces. The PC board is in turn placed on a stage located in the middle of a wind-tunnel test section (Fig. 9). The chip is located near the edge of the PC board, with the hot-wire element located only 1 mm away from the leading edge of the board.

Steady-state output of a infinitely long hot-wire should follow King's half power law, which states that

$$\mathsf{Nu}=A+B\sqrt{\mathsf{R}} \tag{3}$$

where Nu and R are the Nusselt and Reynolds number, respectively; and the terms A and B are constants. We follow the common practice of collapsing the experimental hot-wire data in the form

$$\frac{I^2R_s}{R_s-R_f}=A+BU^n \tag{4}$$

where n=geometric factor; and R_s and R_f=respective sensor resistance at T_s and T_f.

Fig. 10(a) shows a diagram of a constant current driving circuitry. The output voltage of a representative hot wire (150 μm long and 400 μm height) with respect to flow rate under three different levels of biasing is shown in Fig. 11. The level of biasing

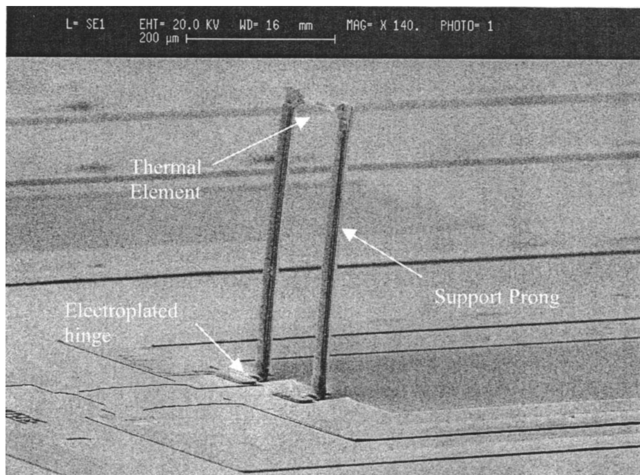

Fig. 6. SEM micrographs of HWA after postrelease strengthening using electroplating

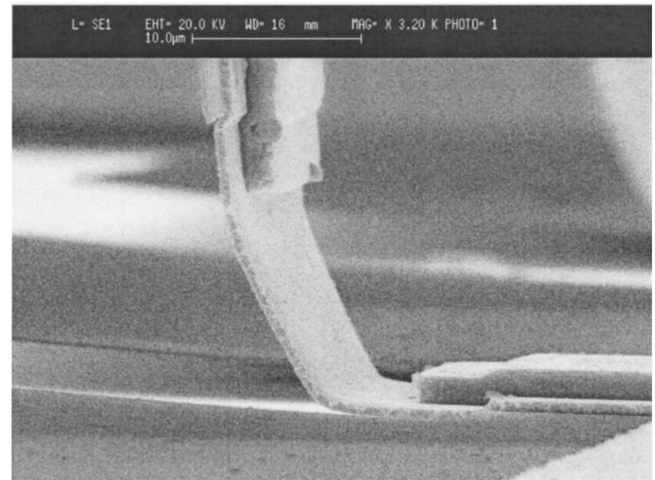

(a)

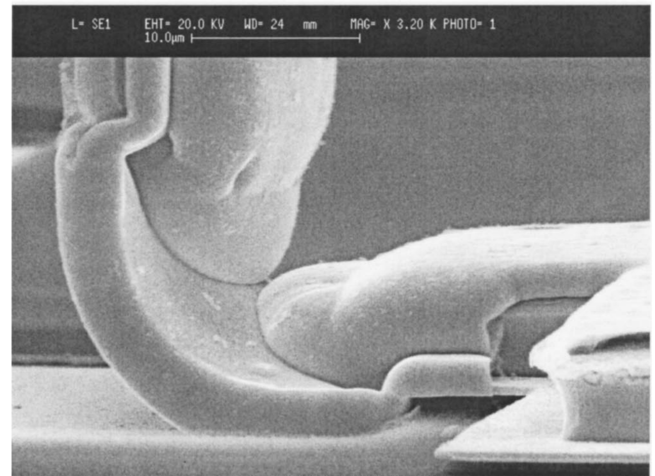

(b)

Fig. 7. SEM graphs of plastically deformed hinge (a) without postrelease Ni plating and (b) with postrelease plating. Reinforced hinge in (b) is significantly thicker than (a).

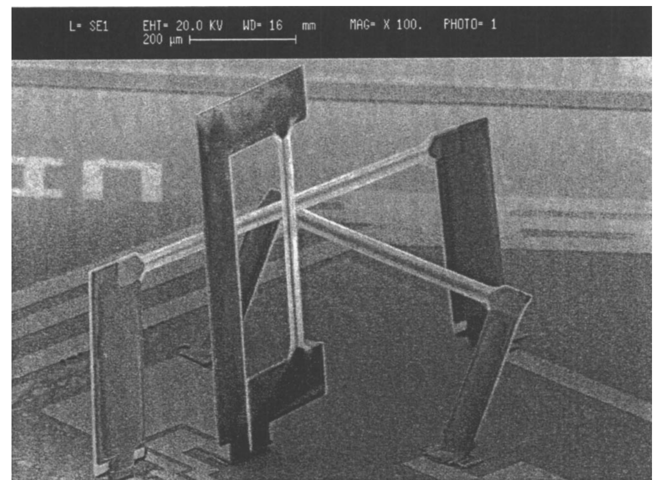

Fig. 8. SEM micrograph of three-component HWA sensor

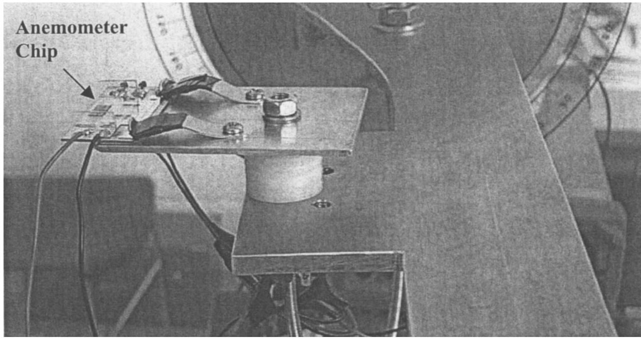

Fig. 9. Photo of wind tunnel measurement setup. Anemometer chip is placed on glass holder, which is positioned on stage located in test section. Finished package is mounted onto test fixture. The yaw angle of chip can be controlled from outside wind tunnel.

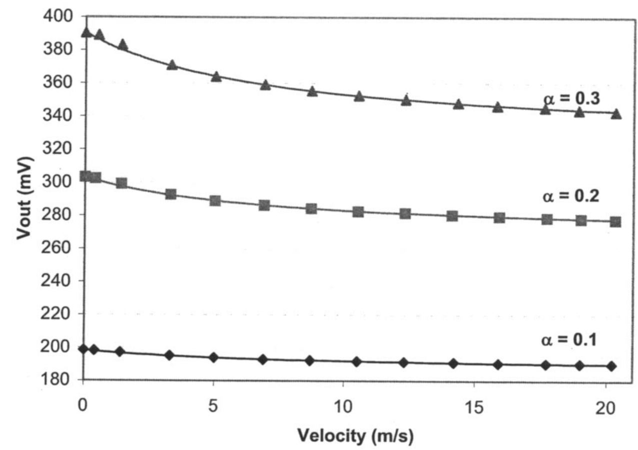

Fig. 11. Response of 600 μm high and 200 μm long, hot-wire anemometer at various overheat ratio (defined at $v=0$ m/s) operating in constant current mode. Solid lines are curve fit using Eq. (4). Air velocity is calibrated using Traceable® hot-wire anemometer.

is defined by the resistive over-heat ratio ($\Delta R/R_0$) within quiescent flow. Due to a positive TCR, the voltage across the hot wire decreases as the flow rate increases. The sensitivity of the output voltage with respect to air velocity increases with an increasing overheat ratio because of the increase in temperature difference between the hot wire and the fluid. Curve fitting with Eq. (4) verifies good correspondence between the measured data and the theoretical relation at velocity above 3 m/s, where n equals 1. At low velocity, because a larger portion of the heat transfer is due to natural convection, the deviation between the data and curve fit is greater. We tested the response of several sensors with different hot-wire length (Fig. 12).

The sensor was also tested under constant temperature (CT) bias using a circuit diagramed in Fig. 10(b). The hot-wire sensor is placed on one leg of a Whetstone bridge. The bridge circuit is balanced when $R_s R_2 = R_1 R_3$. The resistor R_3 is a variable resister used to set the overheat ratio α using the following equation:

$$R_3 = \frac{R_2}{R_1}(1+\alpha) \tag{5}$$

The term R_2/R_1 is also called the bridge ratio. It can be show that the voltage output will vary with flow speed in the relation below.

$$V^2 = A + BU^n \tag{6}$$

where A and B=constants and n again=geometric factor. As Eq. (8) suggests, the CT output is very nonlinear. The CT output response of the same hot wire in the CC test above is shown in Fig. 13. The fitted lines are the theoretical curves ($n=0.8$), and they agree well with the measured data. We tested the response of multiple hot wires at various heights (400, 600, and 1,000 μm). It was found that n decrease from 0.8 for a 400-μm-tall device down to 0.6 for a 1,000-μm-tall device. The reason for this change may be due to the flow interference of the substrate, but it is not known at the moment.

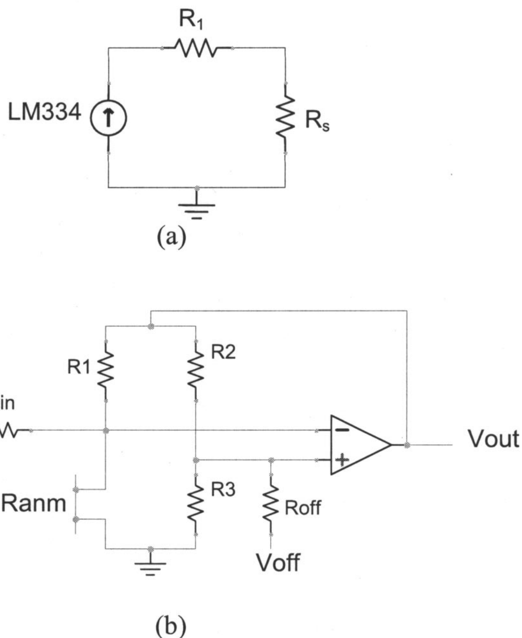

Fig. 10. Schematic of (a) constant current driving circuit and (b) constant temperature circuit. Bridge ratio $n=R_2/R_3=10$, $R_{\mathrm{off}} \gg$Ranm, V_{in} and R_{in} not used during steady-state operation.

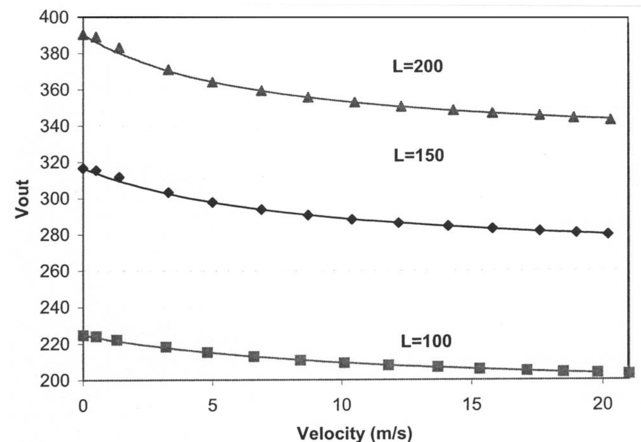

Fig. 12. Response of 400 μm tall hot wires of various lengths operating in constant current mode

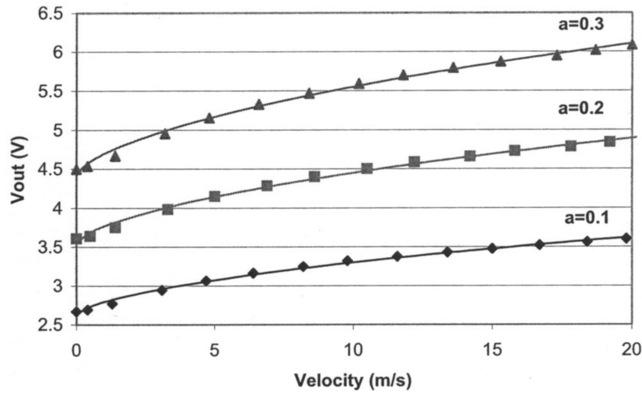

Fig. 13. Response of 400 μm high, 150 μm long, hot-wire anemometer operating in constant temperature mode. Air velocity is calibrated using the Traceable® hot-wire anemometer. Bridge ration of CT circuit is 10, and overheat ratio is set at 0.1, 0.2, and 0.3.

Sensor Time Constant

We characterized the time constant of the thermal element under both constant current and constant temperature conditions. Due to the difficulty in generating a pulsed or step velocity profile with sharp transient, a small signal square wave or sine wave is typically injected into the circuit to act as the disturbance.

Constant Current Mode

In order to obtain a time constant measurement, a disturbance signal is applied to a HWA. We used a representative device with a 150-μm-long hot wire made of 1,200-Å-thick metal filament on a 2.7-μm-thick polyimide. Voltage output with a sinusoidal current input applied to the above-mentioned hot wire is plotted in the frequency domain (Fig. 14). The Bode plot shows only one time constant associated with the −3 dB drop off at 400 Hz. Beyond that frequency, the voltage output drops off at 20 dB/decade.

Constant Temperature Mode

We used two methods to test the transient response in CT operation by feeding sine waves or square waves using the V_{in} supply [Fig. 10(b)]. The schematic diagram of the constant temperature circuit is shown in Fig. 10(b).

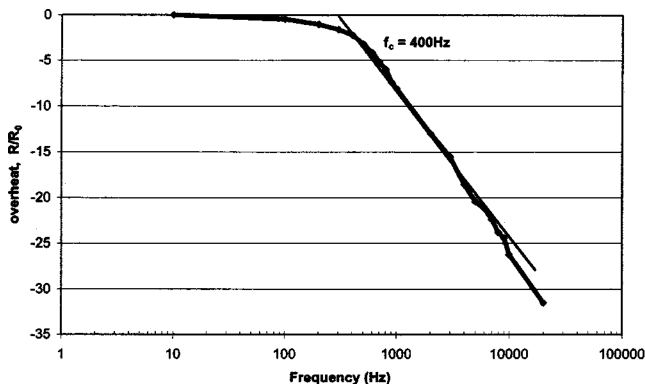

Fig. 14. Resistance change for 150 μm hot wire with a sinusoidal current input of 5.8 mA. Only one time constant was observed in this test. Cutoff frequency at −3 dB point is measured to be around 400 Hz, beyond which signal output drops off at 20 dB/decade.

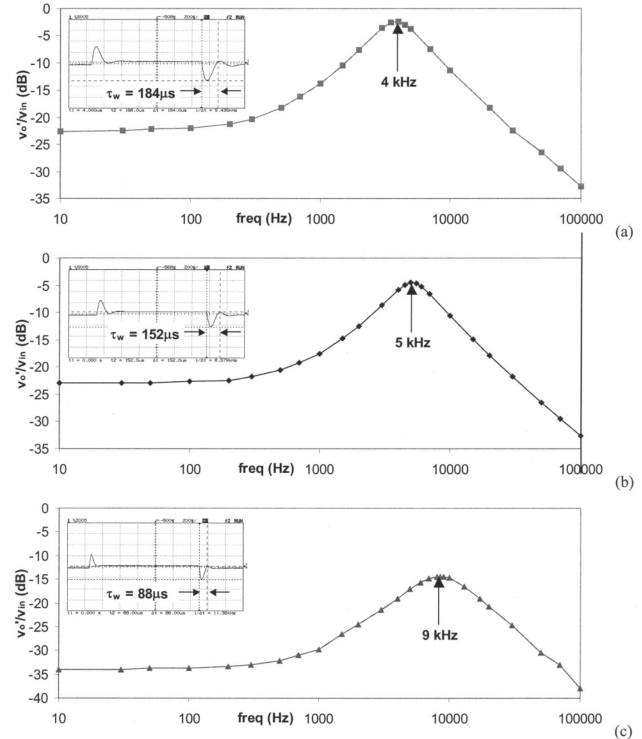

Fig. 15. Frequency response of 200 μm long hot wire in CT mode with sine-wave disturbance under the following conditions: (a) $n=10$, $\alpha=0.3$, vel=2 m/s, (b) $n=10$, $\alpha=0.3$, vel=20 m/s, (c) $n=2$, $\alpha=0.3$, vel=20 m/s. Time constant measured with square wave disturbance is embedded in each figure and corresponds with $f_c=1/(1.3\times\tau_w)$.

Assuming the HWA has only one time constant and the op-amp has a single pole at ω_0, the output voltage is derived (Weidman 1975; Jiang et al. 1994) as a second-order transfer function

$$v_0=\frac{G_v\left(1+\frac{s}{\omega_1}\right)v_{\text{in}}+S_v v}{1+\frac{s}{Q\omega_2}+\left(\frac{s}{\omega_2}\right)^2} \tag{7a}$$

with

$$\omega_1=\frac{1}{(1+2\alpha)\tau} \tag{7b}$$

$$\omega_2=\sqrt{\frac{2\alpha A_0\omega_0}{\tau}\frac{R_2R_3}{(R_2+R_3)^2}} \tag{7c}$$

where G_v=dc voltage gain; S_v=velocity sensitivity defined earlier; Q=quality factor; τ=corner frequency; α=overheat ratio; and A_0 and ω_0=op-amp gain and pole. The responses of the CT circuit with a 200-μm-long HWA to a small signal voltage at a constant velocity are shown in Fig. 15. The value of $V_{\text{out}}/V_{\text{in}}$ is flat up to ω_1, then increases at 20 dB/decade until it reaches a second pole ω_2 at the peak, beyond which it asymptotes at—20 dB/decade.

Using the frequency response plotted in Figs. 15(a and b), we can see that the corner frequency (f_c) increases slightly from 4 to 5 kHz as the velocity is increased. As the bridge ratio decreases [Fig. 15(c)], f_c increases to 9 kHz. However, this is at the expense

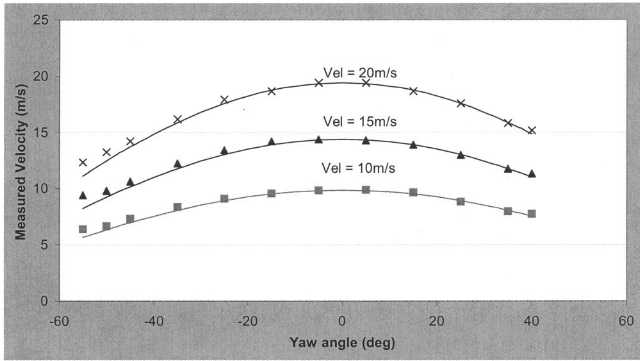

Fig. 16. Yaw angular response of 150 μm high HWA, velocity reading is based on wind tunnel calibration using Eq. (9). Measured data points are placed alongside solid line fitted using cosine law.

of the velocity sensitivity. In order to ensure a flat response, the HWA in CT mode should not operate in turbulence near f_c.

Another way to measure the cutoff frequency is by examining V_{out} with a square wave V_{in}. The square wave test assumes varying the heating current can represent the heating and cooling of the HWA with velocity fluctuation. For example, at the onset of a voltage increase, the feedback circuit will try to balance the bridge by decreasing the voltage output (and hence the heating current); this is similar to a sudden decrease in fluid velocity. The time it takes for V_{out} to settle back to 3% of peak value is defined as τ_w, and can be related to f_c by (Freymuth 1997)

$$f_c = \frac{1}{1.3\tau_w} \tag{8}$$

The corresponding square wave response for each sine wave test is imbedded in the Bode plot with the τ_w clearly marked. The responses from square wave testing verify the cutoff frequency found in all three cases with the sine wave test. This cutoff frequency of new HWA sensors is comparable to that of a commercial anemometer.

Angular Response

The HWA sensor is sensitive to the direction of fluid flow. Provided a sufficiently large aspect ratio for the HWA filament, the yaw response should follow the cosine relation, namely

$$U(\theta) = U_0 \cos(\theta) \tag{9}$$

Testing of the yaw response is done using a rotating stage setup shown in Fig. 9. We used the constant temperature mode here because of the higher-flow sensitivity associated with this mode. In the measurement, HWA output is measured at angle between $-50°$ and $50°$ at $5°$ intervals. The yaw response of the 150-μm-long HWA (Fig. 16) agrees with the cosine relation wells.

Flow Sensors Based on Momentum Transfer

Introduction

Flow sensors based on flow momentum transfer have been reported in the past. The previously reported devices fall into two categories. A first type utilizes monolithic cantilever beams fabricated within the plane of the wafer by using bulk-micromachining methods. Such a sensor is not applicable for large array formation, as each sensor must be discretely packaged. A second sensor type utilizes a vertical, high-aspect-ratio cilium joined with micromachined force-sensing components (Ayers et al. 1998; Ozaki et al. 2000). The overall yield and repeatability of the sensors are generally low at present. For example, one group attached fine bonding wires to micromachined sensors.

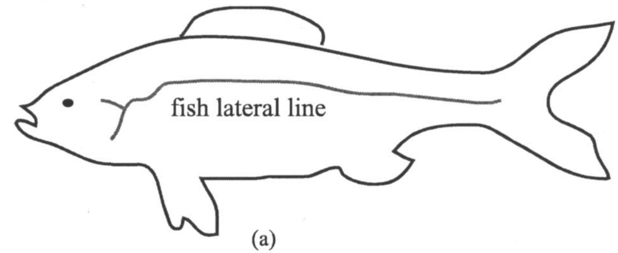

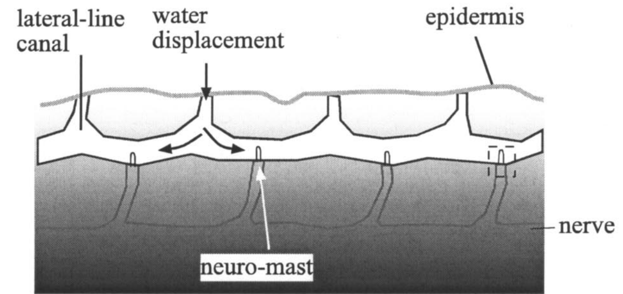

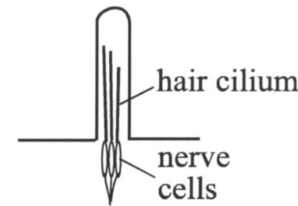

Fig. 17. Schematic diagram of fish lateral line systems. (a) Location of lateral line on surface of fish; (b) enlarged view of segment of the fish lateral line, showing distributed sensors nodes; and (c) schematic diagram of individual neuron node, called neuromast, consisting of cluster of individual hair cells.

We leverage the three-dimensional assembly process to realize a sensor of a second type mentioned above, with much improved process efficiency. The new sensor architecture is inspired by biological sensors. Fish use lateral line sensors to monitor surrounding flow fields for maneuvering and survival under water (Bond 1996). A lateral line system (Fig. 17) consists of an array of distributed sensor nodes (so called neuromasts) that span the length of the fish body. Each sensor node, in turn, consists of a cluster of *hair cells* embedded in protective, gel-like domes [Fig. 17(b)]. An individual biological hair cell, a fundamental mechanoreceptor, consists of a vertical cilium attached to a neuron [Fig. 17(c)]. If the cilium of the hair cell is bent by the local fluid flow, the neuron attached to the cilium stretches and produces action potentials.

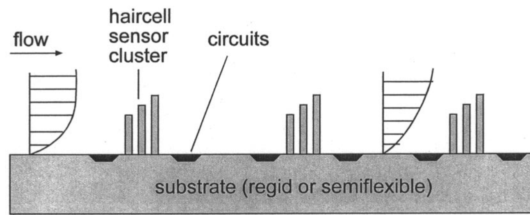

Fig. 18. Schematic diagram of distributed artificial lateral line sensors along surface of underwater vehicle or robot

We have developed flow sensors called artificial hair cell sensors. A proposed system-level implementation of artificial lateral line sensors is shown in Fig. 18. A two-dimensional sensor array consists of many sensor sites, each site consisting of a cluster of sensors with different cilium height and orientation. Sensors at each site provide rich information about two-component flow rate and velocity distribution in the boundary layer.

Sensor Design

Fig. 19 shows the schematic diagram of the artificial lateral line sensor, which consists of an in-plane fixed-free cantilever with a vertical artificial cilium attached at the distal, free end. External flow parallel to the sensor substrate imparts upon the vertical cilium. Due to a rigid connection between the in-plane cantilever and the vertical cilium, a mechanical bending moment is transferred to the horizontal cantilever beam, inducing strain at the base of the cantilever beam. The strain, measured by using piezoresistive sensors embedded at the base of horizontal cantilevers, correlates to the flow rate.

A comprehensive understanding of the relation between the output (relative change of resistance) and the mean flow velocity must take into consideration many possible flow conditions. For complex situations, it may be necessary to use computational fluid dynamics (CFD) method to estimate the sensor output precisely. A comprehensive treatment on the fluid mechanics aspect is beyond the scope of this paper, which focuses on the discussion of new design and fabrication methods. Here, we only briefly discuss the analytical expression of the sensor response (White 1999).

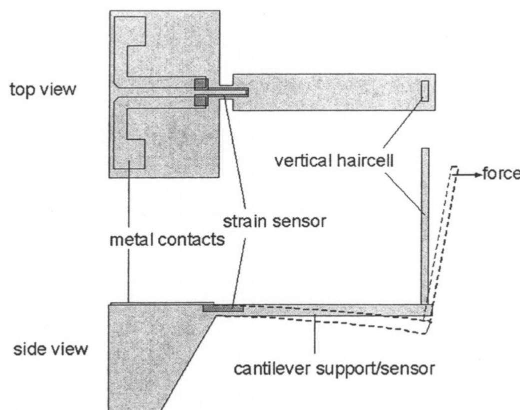

Fig. 19. Schematic diagram of single artificial haircell sensor consisting of horizontal cantilever with vertical cilium attached at free end. We sense bending of vertical cilium using strain sensor located at base of horizontal cantilever.

We denote the mean-stream flow rate as u_0 and the overall length of the cilium as h. The flow velocity is constant beyond the boundary-layer thickness. It is not necessary to completely immerse the sensor in a uniform flow field for the sensor to work properly. Supposing a sensor is located 1 cm away from the leading edge ($x = 0.01$ m), the boundary-layer thickness is approximately 0.94 mm at $u_0 = 0.5$ m/s. In our designs, the height of the cilium is typically less than 1 mm.

The velocity distribution within the boundary layer is a function of the vertical distance y. For example, a generally accepted relationship for low R conditions (laminar boundary layer) is

$$u_y = f(y) = u_0\left(\frac{2y}{\delta} - \frac{y^2}{\delta^2}\right) \tag{10}$$

where τ_w, ρ, and υ = shear stress at the wall, the fluid density, and the kinematic viscosity, respectively. For other flow situations the distribution will be different.

If one assumes that the flow velocity is parallel to the in-plane cantilever, the drag force acting on each slice is

$$F_y = C_D\left(\frac{1}{2}\rho u_y^2 w dy\right) \tag{11}$$

where C_D = local drag coefficient, the value of which depends on R, the hydraulic diameter, and local flow rate; and w = width of the vertical cilium in the direction facing the flow.

One can estimate the moment applied to the horizontal beam by performing finite integration through the length of the vertical cilium, yielding

$$M = \int_{y=0}^{y=h} F_y \times y \tag{12}$$

If the horizontal cantilever has a rectangular cross section with width w_l and thickness t, the expression for the moment of inertia is $I = w_l t^3/12$. Note that w and w_l are not necessarily equal.

The relative change of resistance is given by

$$\frac{\Delta R}{R} = G\varepsilon = G\frac{Mt}{2EI} \tag{13}$$

where the term ε = maximum strain at the cantilever base; E = Young's modulus; and G = lateral gauge factor of the doped piezoresistor. With the velocity profile of Eq. (12), the sensor output is related to the mean flow velocity as

$$\frac{\Delta R}{R} = \frac{3GwC_D\rho\left(\frac{h^4}{\delta^2} + \frac{h^6}{6\delta^4} - \frac{4h^5}{5\delta^3}\right)u_0^2}{Ew_l t^2} \tag{14}$$

Fabrication Process

The overall fabrication process of the artificial hair cell is shown in Fig. 20. We start the process by growing thermal oxide on a silicon wafer. The oxide layer is patterned and selectively removed to provide openings doping. The silicon is doped using a boron source at 950°C for 15 min, forming piezoresistive sensors. The targeted doping concentration is $1.3\times10^{19}\,\mathrm{cm}^{-3}$ and the sheet resistivity of the doped resistor is approximately 100 Ω/□. The gauge factor of such a doped piezoresistive sensor is a function of the doping concentration and the substrate orientation (Pfann and Thurston 1961; Middelhoek and Audet 1989).

Structures that are pertinent to the PDMA process are then deposited and patterned. We deposit a layer of thin-film copper

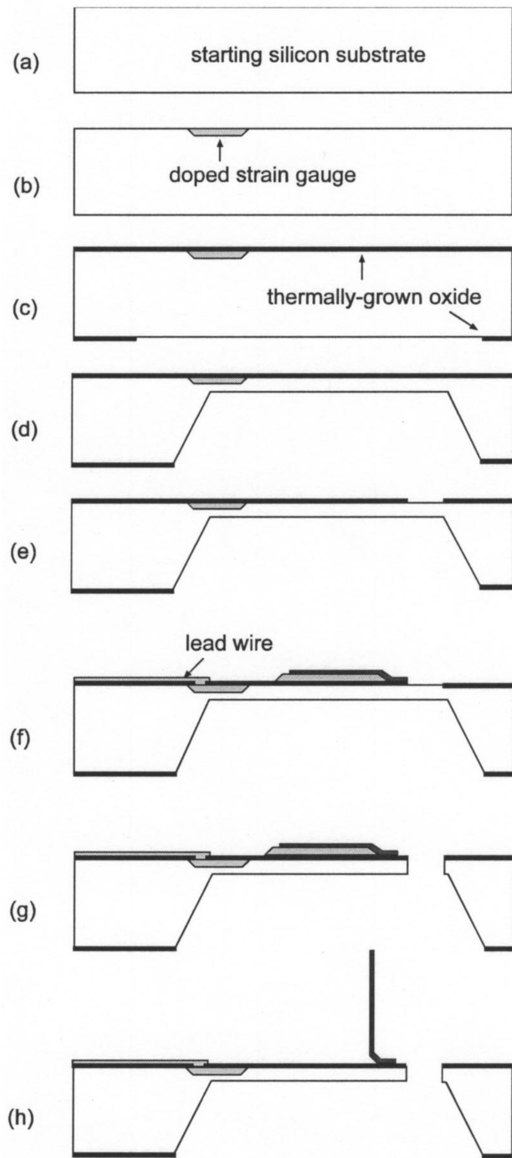

Fig. 20. Fabrication process of artificial lateral line sensor with integrated strain gauges. At final step, vertical cilium is assembled into three-dimensional position. It can be further protected and insulated by uniform, conformal deposition of parylene thin film (Fig. 9).

(300 nm thick) and pattern it photolithographically. A 600-nm-thick gold thin film is deposited by using the liftoff technique. This ensures good step coverage over the boundary of the sacrificial material and minimizes stress concentration. The thickness of the subsequently electroplated Permalloy material is 10 μm. The wafer is etched from the backside using wet anisotropic etching or deep reactive ion etching until a silicon membrane with desired thickness is achieved. Both methods have been implemented successfully although the deep reactive ion etching is preferred because it allows easy control of the thickness of the diaphragm. The thickness of the silicon diaphragm corresponds to the thickness and the moment of inertia of the in-plane cantilever.

The wafer is then etched from the front side to define the cantilever beams. Following this step, the wafer is immersed in diluted HCl solutions to remove the copper sacrificial layer and to free the gold cantilever beam. We then perform the PDMA process by using a piece of permanent magnet that has a magnetic

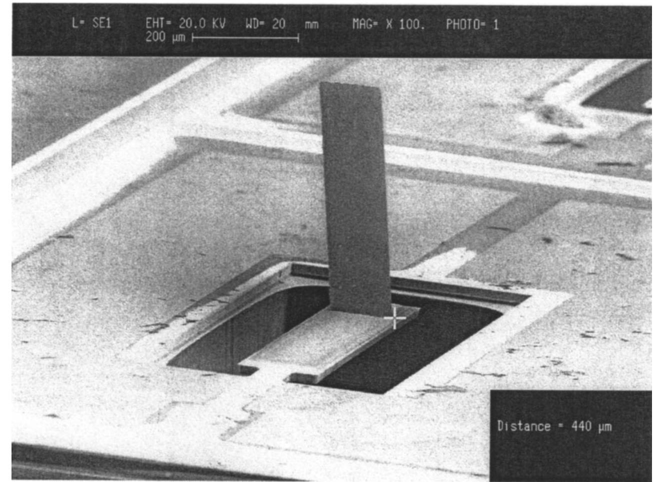

Fig. 21. SEM of single artificial hair cell sensor. Cilium is 820 μm tall. Strain gauge has nominal resistance of 3 kΩ. Strain gauge is 5 μm wide and effectively 150 μm long.

flux intensity of 1,470 g. The wafer is slowly lowered on top of the magnet to permanent deform the metal cantilevers. The SEM micrograph of a representative device is shown in Fig. 21. The length, width, and thickness of the in-plane cantilever are 1,100, 180, and 17 μm, respectively. The height (h), width (w), and thickness of the vertical cilium are 820, 100, and 10 μm, respectively. Fig. 22 shows the details of a plastically bent region. An extended patch made of 10-μm-thick electroplated permalloy is electroplated to overlap with the edge of the sacrificial layer.

The sensor output is related to the direction of the flow. In theory, it is possible to identify the direction of local fluid flow by providing more than two sensors with their cilia pointing in different directions. We have made arrays of sensors with systematically varying frontal orientation and cilium height Fig. 23. The sensor array with different frontal orientation would sense the direction of the flow, whereas the array with different elevation can be used to probe the boundary-layer velocity distribution.

We have demonstrated that it is possible to strengthen the plastically deformed joint of the vertical cilium by using localized electroless plating methods, similar to the hot-wire anemometers.

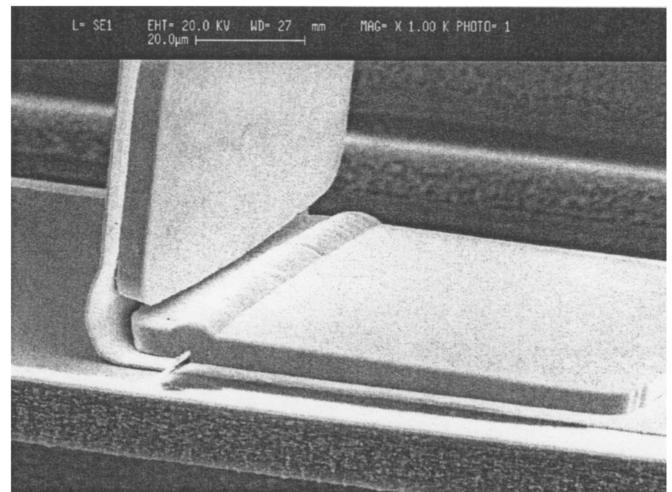

Fig. 22. SEM of plastically bent region at base of vertical cilium

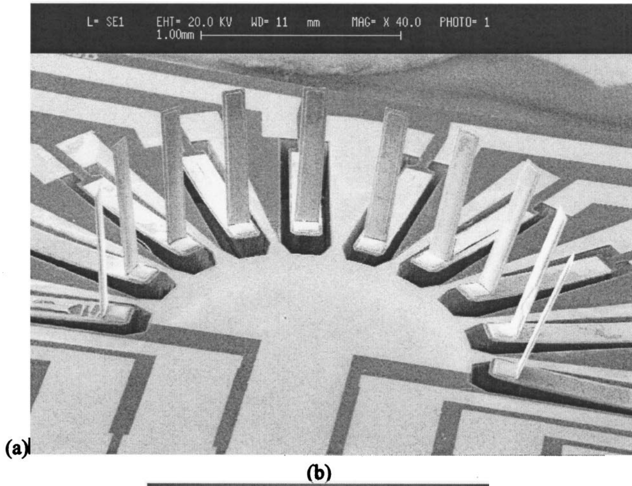

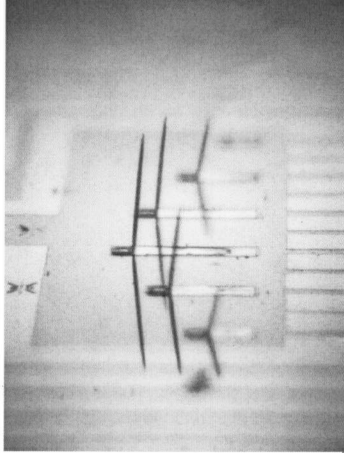

Fig. 23. Array of flow sensors with (a) different frontal orientation and (b) different cilium height

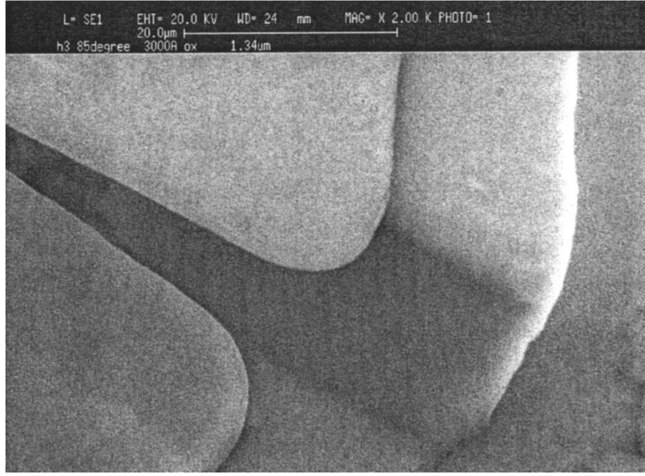

Fig. 25. View of bent region after 1 mm parylene coating

The fabricated device can be further coated with 300-nm-thick uniform parylene deposition for providing electrical insulation and increasing strength (Fig. 24). The parylene film also covers electrical bonding wires (Fig. 25), allowing sensors to operate in conducting fluids without electrolysis or shorting. The deposited material, however, increases the stiffness of the cantilever beam. This is briefly discussed in the following. The effective force constant of a cantilever beam made of a homogeneous material with a Young's modulus of E is approximated by

$$k = \frac{w_l t^3}{3EI} \tag{15}$$

As more parylene is deposited, the value of k will increase due to increased overall thickness. In summary, the thickness of the parylene coating must be optimized with respect to two competing concerns, electrochemical protection and sensitivity.

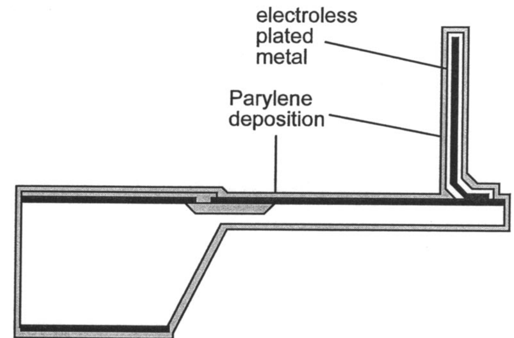

Fig. 24. Schematic diagram of structural strengthening by using electroless plated metal and Parylene. Thickness of layers is not drawn to scale. Thickness of strengthening layers is exaggerated intentionally.

Results and Discussion

We have conducted preliminary flow measurement using the newly developed sensor. Sensors are mounted on a thin glass plate and placed within a laminar flow water tunnel (Fig. 26). One edge of the glass is polished to present a sharp profile facing the flow. The sensor is located 1 mm from the leading (sharp) edge. Laminar flow with u_0 ranging from 0 to 1 m/s passes the sensor element. The flow impacts the cilium at its broad side, i.e., parallel to the long axis of the substrate cantilever. The output response, with the sensor biased under constant voltage (1 V), is shown in Fig. 27. The best-fit curve follows a second-order polynomial expression, as expected from earlier analysis.

Extensive fluid characterization including the robustness of the sensor and performance of arrayed sensors is currently underway.

Conclusions

We have designed and developed efficient microfabrication processes for realizing micromachined flow sensor array with high-

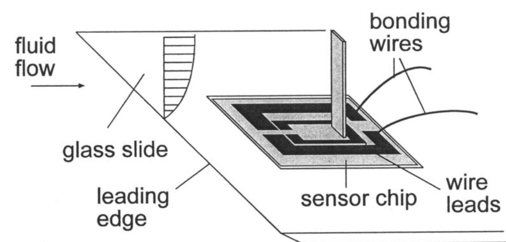

Fig. 26. Schematic diagram of packaged sensor in fluid flow environment

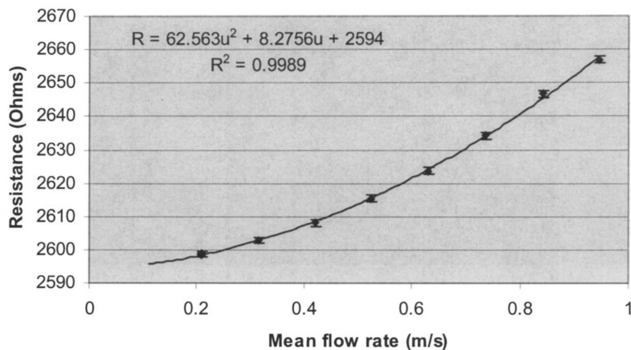

Fig. 27. Measurement results showing output current versus flow rate of representative sensor under constant voltage biasing

spatial resolution—one based on the thermal transfer principle and another on the momentum transfer principle.

A hot-wire anemometer can be fabricated using nonsilicon materials and hence can be potentially produced with low costs and high-fabrication efficiency. The HWA can potentially be realized in large array format for distributed flow sensing. If necessary, the sensor can be made on flexible substrates for conformal coating of fluid dynamic surfaces of interests. The sensor has been systematically characterized under both constant current and constant temperature modes. The time constant of a sensor is 400 Hz under constant current mode and 10 kHz under constant temperature mode.

We have developed the design and fabrication process of an individual micromachined artificial lateral-line sensor for flow sensing applications. The sensor is realized using combined bulk-micromachining methods and an efficient three-dimensional assembly method. Sensors can be strengthened using electroless plating and parylene conformal coating. They can be realized monolithically using combined bulk-micromachining and three-dimensional assembly methods.

Acknowledgments

This work is conducted with funding provided by the U.S. Air Force Office of Scientific Research (AFOSR) under the Bioinspired Concept (BIC) program, the National Science Foundation (NSF) CAREER program, and NASA. The writers wish to acknowledge the technical support of John Hughes, Hal Romans, and Richard Blaney for maintaining processing equipment at the Micro and Nanotechnology Laboratory of the University of Illinois, and Andy Broeren at the Department of Aeronautical and Astronautical Engineering at University of Illinois. J.C. and Z.F. made equal contributions to this work.

Reference

Ayers, J., Zavracky, P. M., McGruer, N., Massa, D., Vorus, V., Mukherjee, and R., Currie, S. (1998). "A modular behavioral-based architecture for biomimetic autonomous underwater robots." *Proc., Autonomous Vehicles in Mine Countermeasures Symposium*, Naval Postgraduate School, (CD-Rom), world wide web site ⟨http://www.cis.plym.ac.uk/cis/InsectRobotics/biomimetics.htm⟩ (1998).

Blackwelder, R. F. (1981). *Methods of experimental physics: Fluid dynamics*, Vol. 18, Part A, Academic, New York, 99–154.

Boillat, M. A., van der Wiel, A. G., Hoogerwerf, A. C., and de Rooij, N. F. (1995). "A differential pressure liquid flow sensor for flow regulation and dosing systems." *Proc., IEEE Micro Electro Mechanical Systems*, 350–2.

Bond, C. E. (1996). *Biology of fishes*, 2nd Ed., Saunders, Philadelphia.

Brunn, H. H. (1995). *Hot-wire anemometry: Principles and signal analysis*, Oxford University Press, New York.

de Bree, H. E., Jansen, H. V., Lammerink, T. S. J., Krijnen, G. J. M., and Elwenspoek, M. (1999). "Bi directional fast flow sensor with a large dynamic range." *J. Micromech. Microeng.,* 9(2), 186–9.

Dittmann, D., Ahrens, R., Rummler, Z., Schlote-Holubek, K., and Schomberg, W. K. (2001). "Low-cost flow transducer fabricated with the AMANDA-process." *11th Int. Conf. on Solid-State Sensors and Actuators*, Munich, Germany, June 10–14, 1472–1475.

Ebefors, T., Kalvesten, E., and Stemme, G. (1998). "Three dimensional silicon triple-hot-wire anemometer based on polyimide joints." *Proc. Eleventh Annual Int. Workshop on Micro Electro Mechanical Systems. An Investigation of Micro Structures, Sensors, Actuators, Machines and Systems*, 93–8.

Enoksson, P., Stemme, G., and Stemme, E. (1996). "A Coriolis mass flow sensor structure in silicon." *Proc., 9th Annual Int. Workshop on Micro Electro Mechanical Systems. An Investigation of Micro Structures, Sensors, Actuators, Machines and Systems*, 156–61.

Freymuth, F. (1977). "Frequency response and electronic testing for constant temperature hot-wire anemometers." *J. Phys. E*, 10.

Goldstein, R. J. (1983). *Fluid mechanics measurements*, Hemisphere, Washington.

HD Microsystems. (1998). "Pyralene polyimide coating for electronics: PI2610 series—Product information and process guidelines." HD Microsystems.

Jiang, F., Tai, T. C., Ho, C. M., Rainer, K., and Garstenauer, M. (1994). "Theoretical and experimental studies of micromachined hot-wire anemometer." *Digest IEEE Int. Electron Devices Meetings (IEDM)*, 139–142.

Kalvesten, E., Vieider, C., Lofdahl, L., and Stemme, G. (1996). "An integrated pressure-flow sensor for correlation measurements in turbulent gas flows." *Sens. Actuators A,* A52(1–3), 51–8.

Kovacs, G. T. A. (1998). *Micromachined transducers sourcebook*, McGraw-Hill, New York.

Lofdahl, L., Kalvesten, E., Hadzianagnostakis, T., and Stemme, G. (1996). "An integrated silicon based wall pressure-shear stress sensor for measurements in turbulent flows." *Proc., 1996 Int. Mechanical Engineering Congress and Exposition*, 245–51.

Lofdahl, L., Stemme, G., and Johansson, B. (1992). "Silicon based flow sensors used for mean velocity and turbulence measurements." *Exp. Fluids,* 12(4–5), 270–6.

Lomas, C. G. (1986). *Fundamentals of hot wire anemometry*, Cambridge University Press, Cambridge, England.

Middelhoek, S., and Audet, S. A. (1989). *Microelectronics and signal processing: Silicon sensors*, Academic, New York.

Neda, T., Nakamura, K., and Takumi, T. (1996). "A polysilicon flow sensor for gas flow meters." *Sens. Actuators A,* 54, 621–31.

Ozaki, Y., Ohyama, T., Yasuda, T., and Shimoyama, I. (2000). "An air flow sensor modeled on wind receptor hairs of insects." *Proc., MEMS 2000*, 531–6.

Padmanabhan, Goldberg, H., Breuer, K. D., and Schmidt, M. A. (1996). "A wafer-bonded floating-element shear stress microsensor with optical position sensing by photodiodes." *J. Microelectromech. Syst.,* 5(4), 307–15.

Perry, A. E. (1982). *Hot wire anemometry*, Clarendon, Oxford, England.

Pfann, W. G., and Thurston, R. N. (1961). "Semiconducting stress transducers utilizing the transverse and shear piezoresistance effects." *J. Appl. Phys.,* 32(10), 2008–19.

Rediniotis, O. K., and Vijayagopal, R. (1999). "Miniature multihole pressure probes and their neural-network-based calibration." *AIAA J.,* 37(6), pp. 666–74.

Richter, M., Wackerle, M. Woias, P., and Hillerich, B. (1999). "A novel

flow sensor with high time resolution based on differential pressure principle.'' *Proc., 12th Int. Conf. on Micro Electro Mechanical Systems*, Orlando, Fla. 118–123.

Svedin, N., Kalvesten, E., Stemme, E., and Stemme, G. (1998). ''A new silicon gas-flow sensor based on lift force.'' *J. Microelectromech. Syst.,* 7(3), 303–308.

Svedin, N., Stemme, E., and Stemme, G. (2001). ''A static turbine flow meter with a micromachined silicon torque sensor.'' *Technical Digest, MEMS 2001, 14th IEEE Int. Conf. on Micro Electro Mechanical Systems*, Interlaken, Switzerland, 208–211.

van Baar, J. J., Wiegerink, R. J., Lammerink, T. S. J., Krijnen, G. J. M., and Elwenspoek, M. (2001). ''Micromachined structures for thermal measurements of fluid and flow parameters.'' *J. Micromech. Microeng.,* 11(4), 311–8.

van der Wiel, A. J., Boillat, M. A., and de Rooij, N. F. (1995). ''A bi-directional silicon orifice flow sensor characterised for fluid temperature and pressure.'' *Proc., 8th Int. Conf. on Solid-State Sensors and Actuators and Eurosensors IX*, Vol. 2, 420–3.

van der Wiel, A. J., Linder, C., de Rooij, N. F., and Bezinge, A. (1993). ''A liquid velocity sensor based on the hot-wire principle.'' *Sens. Actuators A,* A37–38, 693.

van Honschoten, J. W., Krijnen, G. J. M., Svetovoy, V. B., de Bree, H. E., and Elwenspoek, M. C. (2001). ''Optimization of a two wire thermal sensor for flow and sound measurements.'' *Proc., 14th Int. Conf. Micro Electro Mechanical Systems (MEMS'2001)*, 523–526

Weidman, P. D., and Browand, F. K. (1975). ''Analysis of a simple circuit for constant temperature anemometry.'' *J. Phys. E,* 8(2), 553–560.

White, F. M. (1999). *Fluid mechanics*, 4th Ed., McGraw-Hill, New York.

Xu, Y., Jiang, F., Lin, Q., Clendenen, J., Tung, S., and Tai, Y. C. (2002). ''Under water shear stress sensor.'' *Proc., 15th IEEE Int. Conf. on Micro Electro Mechanical Systems (MEMS'02)*.

Zou, J., Chen, J., and Liu, C. (2001). ''Plastic deformation magnetic assembly (PDMA) of out-of-plane microstructures: Technology and application.'' *IEEE/ASME J. MEMS,* 10(2), 302–309.